Microscopic calculation of the electron–optical-phonon interaction in ultrathin $GaAs/Al_xGa_{1-x}As$ alloy quantum-well systems

Insook Lee and S. M. Goodnick
Department of Electrical and Computer Engineering, Oregon State University, Corvallis, Oregon 97331

M. Gulia and E. Molinari
Dipartimento di Fisica, Università di Modena, I-41100 Modena, Italy

P. Lugli
Dipartimento di Ingegneria Elettronica, Università di Roma "Tor Vergata," I-00173 Roma, Italy
(Received 11 July 1994; revised manuscript received 2 September 1994)

We have calculated electron–optical-phonon scattering rates in ultrathin $GaAs/Al_xGa_{1-x}As$ alloy quantum-well systems of finite depth, based on a fully microscopic lattice dynamics approach for the phonon spectra. A pseudo-unit-cell model is utilized to calculate the lattice-dynamical properties of the $Al_xGa_{1-x}As$ alloy system together with the two-parameter Keating potential and the long-range Coulomb potential between ions. The polar interactions of quantum-confined electrons with GaAs- and AlAs-like optical modes are presented for both intrasubband and intersubband transitions, and the comparison with other theoretical calculations made. Good agreement is obtained for the $1\rightarrow1$ and $2\rightarrow1$ transition rates between the microscopic pseudo-unit-cell model and a macroscopic two-pole dielectric continuum model.

I. INTRODUCTION

The electron–optical-phonon (e-ph) interaction in quantum wells (QW's) and superlattices (SL's) is a topic of continuing interest, since the transport properties of high-speed heterostructure devices are primarily governed by the carrier interactions with phonons. The presence of heterointerfaces may give rise to the confinement of optical phonons in the layers and the localization in the vicinity of interfaces. Therefore, the e-ph interactions in heterostructures may differ from those in the bulk materials, particularly in QW's having very thin well width and ultrathin-layered SL's.

Several approaches have been applied to calculate e-ph scattering rates in heterostructures.[1] Recently, a fully microscopic calculation was reported for GaAs/AlAs systems by Rücker *et al.*[2] on the basis of *ab initio* phonon spectra.[3] Although a great majority of heterostructures contain alloy semiconductors, the existing microscopic theoretical treatments of e-ph scattering probabilities are limited to binary/binary material systems. This limitation is due to the fact that in general, accurate microscopic studies of alloy SL's require large supercells to simulate alloy disorder,[3] and, therefore, the subsequent Calculation of e-ph rates becomes intractable, even for relatively thin SL's.

The purpose of this paper is to investigate the e-ph interaction in $GaAs/Al_xGa_{1-x}As$ alloy QW's, based on a different fully microscopic approach to the lattice dynamics of the alloy. The $GaAs/Al_xGa_{1-x}As$ alloy system is of great importance for many high-speed electronics and optoelectronic devices because the lattice mismatch between GaAs and $Al_xGa_{1-x}As$ is extremely small (less than 0.15% at 300 K), such that the concentration of undesirable interface states is negligible. In this respect, $Al_xGa_{1-x}As$ alloys have been studied as prototypical ternary materials. Their long-wavelength optical phonons display a two-mode behavior throughout the whole composition range and have well-defined dispersive character.[4,5] As mentioned above, modeling alloys to study lattice-dynamical properties, without using any mean-field approximations (average-t-matrix,[6] coherent potential,[7] etc.), requires the introduction of large supercells to treat the disorder. We have proposed a simpler technique based on the pseudo-unit-cell concept reported by Chang and Mitra in 1971,[8] instead of using a huge supercell, and our results have been presented.[9] Related works by Bechstedt *et al.*[10,11] have recently appeared which follow a similar approach to calculate the lattice dynamics in heterostructure alloy systems. This model has proven to be a simple approach to calculate general features of the lattice-dynamical properties of alloys. However, since the pseudo-unit-cell model imposes translational invariance in the mixed crystal system, it contains no information on alloy disorder effects such as broadening or alloy scattering. In this paper, we use this simple model for the lattice dynamics of alloys to calculate the e-ph interaction in the alloy QW system. Since our calculation is in the framework of three-dimensional dynamics, the theory is not restricted to long-wavelength modes nor certain phonon propagation directions. Our results are compared with the results using a macroscopic theory of phonon modes based on the dielectric continuum model (DCM). In Sec. II, the general formal setup for the calculation of electron–optical-phonon interactions is illustrated. We describe our microscopic calculation of phonons in Sec. III. Results and discussions on the scattering rates in QW's are presented in Sec. IV. As an application of the technique, numerical results are given for a $GaAs/Al_{0.3}Ga_{0.7}As$ alloy QW sys-

tem and compared to the results obtained using the DCM (Sec. V). Finally, Sec. VI contains our conclusions.

II. ELECTRON–OPTICAL-PHONON INTERACTION IN QW's

For the polar interaction of quantum-confined electrons with phonons, the interaction Hamiltonian $H_{e\text{-ph}}$ is given by $-e\varphi$, where e is the electron charge and φ is the electrostatic potential associated with the lattice vibrations.[12] In a quantum-well (QW) grown along the z direction, the total scattering rate of an electron with in-plane wave vector $\mathbf{k}_\parallel$ from subband i to subband j, making use of Fermi's golden rule, is obtained as follows (assuming parabolic bands):[13]

$$\begin{aligned}\Gamma_{ij}(\mathbf{k}_\parallel) &= \frac{2\pi}{\hbar}\sum_{\mathbf{k}'_\parallel} |\langle n_q \pm 1; \mathbf{k}'_\parallel, j | H_{e-\text{ph}} \mid n_q; \mathbf{k}_\parallel, i\rangle|^2 \delta\left(\frac{\hbar^2 k'^2_\parallel}{2m^*} - \frac{\hbar^2 k^2_\parallel}{2m^*} \pm \hbar\omega^*\right) \\ &= \frac{2\pi e^2}{\hbar}\sum_{\mathbf{k}'_\parallel,\nu}\begin{pmatrix} n_{q\nu}+1 \\ n_{q\nu}\end{pmatrix} \mid g^\nu_{ij}(\mathbf{q}_\parallel)\mid^2 \delta\left(\frac{\hbar^2 k'^2_\parallel}{2m^*} - \frac{\hbar^2 k^2_\parallel}{2m^*} \pm \hbar\omega^*\right) \\ &= \frac{m^* A e^2}{2\pi\hbar^3}\sum_{\nu}\begin{pmatrix} n_{q\nu}+1 \\ n_{q\nu}\end{pmatrix}\int_0^{2\pi} d\theta \mid g^\nu_{ij}(\sqrt{k'^2_0 + k^2_\parallel - 2k'_0 k_\parallel \cos\theta}) \mid^2, \end{aligned} \tag{1}$$

where $\mathbf{k}'_\parallel$ is equal to $\mathbf{k}_\parallel \pm \mathbf{q}_\parallel$ and the plus (minus) sign is for phonon absorption (emission). m^* is the effective mass of the conduction band, A is the in-plane normalization area, and $n_{q\nu}$ is the Bose function for the phonon occupation, which is given by

$$n_{q\nu} = \frac{1}{e^{\frac{\hbar\omega_\nu(\mathbf{q}_\parallel)}{k_B T}} - 1}. \tag{2}$$

The term $\hbar\omega^*$ appearing in the energy-conserving δ function satisfies the relation

$$\pm\hbar\omega^* = \pm\hbar\omega_\nu + (E_j - E_i), \tag{3}$$

where $(E_j - E_i)$ is the energy difference between the final and initial electronic subbands. In the last line of Eq. (1), integration over all possible $\mathbf{k}'_\parallel$ has been performed and k'^2_0 is defined as

$$k'^2_0 = k^2_\parallel \mp \frac{2m^*\omega^*}{\hbar}. \tag{4}$$

The coupling factor g_{ij} is given by the overlap integral,

$$g^\nu_{ij}(\mathbf{q}_\parallel) = \int \xi^*_j(z)\varphi^\nu_{\mathbf{q}_\parallel}(z)\xi_i(z)dz. \tag{5}$$

Here, $\xi_i(z)$ is the normalized envelope function of the ith quantized electron state, the solution of Schrödinger's equation within the effective-mass approximation,[14] and $\varphi^\nu_{\mathbf{q}_\parallel}(z)$ is the potential associated with the quantized phonon mode ν. By symmetry arguments, g_{ij} is nonzero only for phonons with symmetric potentials for intrasubband scattering ($i = j$), whereas phonons with antisymmetric potentials contribute to the intersubband scattering ($i \neq j$).

III. CALCULATION OF PHONONS IN ALLOY SEMICONDUCTORS AND SL's

We start from a recent calculation[15] of the phonon spectra of polar semiconductor SL's, based on the two-parameter Keating potential[16] and the long-range Coulomb interaction between ions, which was shown to reproduce the characteristic features of the phonon spectra in these systems. The short-range Keating potential for the crystal is expressed in the following form:

$$\begin{aligned}\Phi = \frac{1}{2}\sum_\ell \Bigg[&\sum_{\kappa'} \frac{3\alpha_{\kappa\kappa'}}{4d^2_{\kappa'}}\{\mathbf{x}_{\kappa\kappa'}(\ell)\cdot\mathbf{x}_{\kappa\kappa'}(\ell) - d^2_{\kappa'}\}^2 \\ &+ \sum_{\kappa=1}^{n}\sum_{\kappa',\kappa''>\kappa'} \frac{3\beta_{\kappa\kappa'\kappa''}}{4d^2_{\kappa'\kappa''}}\Bigg\{\mathbf{x}_{\kappa\kappa'}(\ell)\cdot\mathbf{x}_{\kappa\kappa''}(\ell) \\ &+ \frac{d^2_{\kappa'\kappa''}}{3}\Bigg\}^2\Bigg], \end{aligned} \tag{6}$$

where $\mathbf{x}_{\kappa\kappa'}(\ell) = \mathbf{x}(\ell\kappa') - \mathbf{x}(0\kappa)$ is the bond vector from atom κ to atom κ' in the ℓth unit cell, $d_{\kappa'}$ is the equilibrium bond length, and $\alpha_{\kappa\kappa'}$ is the bond-stretching force constant between the two atoms. $\beta_{\kappa\kappa'\kappa''}$ is the bond-bending force constant between the bonds centered at the atom κ and $d^2_{\kappa'\kappa''}$ is the product of $d_{\kappa'}$ and $d_{\kappa''}$. Summations κ' and κ'' are taken over all nearest-neighbor bonds and n represents the number of atoms in the unit cell.

The values of α and β for bulk GaAs were fit to existing experimental data.[15] For AlAs, α and β were assumed for simplicity to be equal to those of GaAs. The resulting AlAs longitudinal optical (LO) phonon dispersion[15] is significantly overestimated with respect to *ab initio* calculations,[17,18] which were recently confirmed by second-order Raman scattering experiments.[19,20] This approximation has some minor implications for the calculated scattering rates, as will be discussed in Sec. IV.

The long-range Coulomb interaction can be calculated exactly by using the conventional Ewald method[21] with an effective charge e^*. The effective charge parameter $Z(=\frac{e^*}{\sqrt{\epsilon_\infty}})$ is determined so as to reproduce the experimental splitting of the LO and transverse optical (TO) phonon frequencies of the bulk materials at the Γ point.

The bulk optical bands of GaAs and AlAs do not overlap, so in a layered structure made of these materials, the

optical modes are well confined within the parent crystal slab and dispersionless, whereas acoustic modes are extended.[22] As an example, the calculated phonon dispersion curves of the $(GaAs)_2/(AlAs)_2$ superlattice (SL) along the growth direction are shown in Fig. 1, using the bulk parameters given in Table I.[23] It is assumed that all the force constant parameters in the superlattice are the same as those in the corresponding bulk materials, except the effective charge parameter at the As interface plane, which is determined by the average of the two constituent bulk values.[15]

For ternary mixed crystals, the introduction of a large supercell is usually required in order to simulate the effect of disorder in alloys. In the present work, we take the simple pseudo-unit-cell concept[8] to study the lattice-dynamical properties of alloys instead of using a huge supercell. In a mixed $A_xB_{1-x}C$ crystal, where $0 \leq x \leq 1$, the A and B ions are assumed to be distributed randomly in their corresponding sublattice with a uniform distribution (i.e., with no clustering). The pseudo-unit-cell is formed by ions xA, $(1-x)B$, and C, and this unit cell is repeated in a mixed crystal. Probabilistically, the pseudo-unit-cell may be thought of as a configurational average unit cell. The fractional amounts of the A and B ions located at the same sublattice site are proportional to the concentrations and the corresponding forces involving these ions are weighted by these factors.[8,24]

Utilizing the pseudo-unit-cell model together with the two-parameter Keating potential and the long-range Coulomb interaction for the potential between the ions,

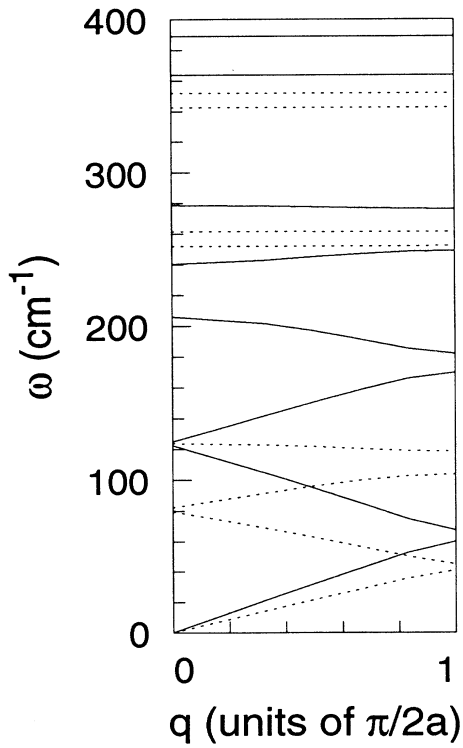

FIG. 1. Phonon dispersion relations of the $(GaAs)_2/(AlAs)_2$ SL along the growth direction. The solid (dotted) lines show longitudinal (transverse) modes.

TABLE I. Bulk parameters used in the phonon calculations. The masses of the cations and anions are denoted by m_c and m_a, respectively, α and β are the bond-stretching and the bond-bending force constants, respectively, in units of N/m, Z is the effective charge parameter, and l and a are the equilibrium bond length and lattice constant, respectively, in atomic units.

	m_c	m_a	α	β	Z	l	a
GaAs	69.72	74.92	36.18	3.96	0.664	4.626	10.68
AlAs	26.98	74.92	36.18	3.96	0.78	4.626	10.68

the lattice dynamical properties of $Al_xGa_{1-x}As$ can be calculated within the three-dimensional framework.[9] The equation of motion for the ionic displacement $\mathbf{u}(\ell\kappa)$ of the ion κ in the unit cell ℓ in the mixed crystal may be written[21]

$$M_\kappa \ddot{u}_\alpha(\ell\kappa) = -\sum_{\ell'\kappa'\beta} c(\kappa')\Phi_{\alpha\beta}(\ell\kappa;\ell'\kappa')u_\beta(\ell'\kappa'), \tag{7}$$

where M_κ is the mass of the κth atom, and $u_\alpha(\ell\kappa)$ and $u_\beta(\ell\kappa)$ are the α- and β-Cartesian components of $\mathbf{u}(\ell\kappa), \alpha, \beta = x, y, z$, respectively. $\ddot{u}_\alpha(\ell\kappa)$ is the second derivative of $u_\alpha(\ell\kappa)$ with respect to time and $c(\kappa')$ denotes the concentration of the atom κ', i.e., $c(Al) = x$, $c(Ga) = 1 - x$, and $c(As) = 1$. Φ is the interaction potential of the crystal (6) and

$$\Phi_{\alpha\beta}(\ell\kappa;\ell'\kappa') = \left.\frac{\partial^2\Phi}{\partial u_\alpha(\ell\kappa)\partial u_\beta(\ell'\kappa')}\right|_0, \tag{8}$$

where the subscript zero means that the derivative is evaluated in the equilibrium configuration. To obtain a more natural set of equations with a symmetric force matrix,[24] Eq. (7) can be multiplied by $c(\kappa)$. Assuming that the displacement $\mathbf{u}(\ell\kappa)$ is a traveling wave of the form

$$\mathbf{u}(\ell\kappa) = \frac{\mathbf{w}(\kappa)}{\sqrt{c(\kappa)M_\kappa}} e^{i[\mathbf{k}\cdot\mathbf{x}(\ell\kappa)-\omega t]}, \tag{9}$$

the equation of motion (7) becomes

$$[\mathbf{C} - \omega^2\mathbf{I}][\mathbf{w}] = 0. \tag{10}$$

$\mathbf{I}$ is the identity matrix and $\mathbf{w}$ is a 1×9 column matrix. The dynamical matrix $\mathbf{C}$ is a 9×9 Hermitian matrix, the elements of which are of the form

$$C_{\alpha\beta}(\kappa\kappa' \mid \mathbf{k}) = \frac{1}{\sqrt{c(\kappa)c(\kappa')M_\kappa M_{\kappa'}}} \sum_{\ell'} c(\kappa)c(\kappa') \times \Phi_{\alpha\beta}(\ell\kappa;\ell'\kappa')e^{-i\mathbf{k}\cdot[\mathbf{x}(\ell\kappa)-\mathbf{x}(\ell'\kappa')]}. \tag{11}$$

It is assumed that the bond-stretching force constant α and the effective charge parameter Z vary linearly with concentration[24,25] as

$$\alpha_{GaAs}(x) = [1 - \theta_{GaAs}(1-x)]\alpha^0_{GaAs}, \tag{12}$$

$$\alpha_{AlAs}(x) = (1 - \theta_{AlAs}x)\alpha^0_{AlAs}, \tag{13}$$

$$Z_{Ga}(x) = [1 - \lambda_{Ga}(1-x)]Z^0_{Ga}, \tag{14}$$

where x represents the Al mole fraction in the al-

loy. $\alpha^0_{\mathrm{GaAs}}, \alpha^0_{\mathrm{AlAs}}$, and Z^0_{Ga} are determined so that $\alpha_{\mathrm{GaAs}}(0), \alpha_{\mathrm{AlAs}}(1)$, and $Z_{\mathrm{Ga}}(0)$ are the corresponding bulk values. Values of the parameter $\theta_{\mathrm{GaAs}}, \theta_{\mathrm{AlAs}}$, and λ_{Ga} are determined to fit the experimental optical-phonon frequencies at the long-wavelength limit. Then the bond-stretching force constants of $\mathrm{Al}_x\mathrm{Ga}_{1-x}\mathrm{As}$ are weighted in the obvious manner as follows:

$$\alpha^w_{\text{Ga-As}} = (1-x)\alpha_{\mathrm{GaAs}}(x), \tag{15}$$

$$\alpha^w_{\text{Al-As}} = x\alpha_{\mathrm{AlAs}}(x), \tag{16}$$

where α^w's are the weighted bond-stretching force constants. The weighted bond-bending force constants β^w are also determined by

$$\beta^w_{\mathrm{Ga}_{1-x}\mathrm{AsAs}} = (1-x)\beta, \tag{17}$$

$$\beta^w_{\mathrm{AsGa}_{1-x}\mathrm{Ga}_{1-x}} = (1-x)^2\beta, \tag{18}$$

$$\beta^w_{\mathrm{Al}_x\mathrm{AsAs}} = x\beta, \tag{19}$$

$$\beta^w_{\mathrm{AsAl}_x\mathrm{Al}_x} = x^2\beta, \tag{20}$$

$$\beta^w_{\mathrm{AsAl}_x\mathrm{Ga}_{1-x}} = x(1-x)\beta\ , \tag{21}$$

where $\beta = \beta_{\mathrm{GaAs}} = \beta_{\mathrm{AlAs}}$. Note that these weighted force constants already imply the $c(\kappa)$'s in the summation in Eq. (11). We fit the effective charge parameter $Z_{\mathrm{Ga}}(x)$ to reproduce the GaAs-like LO and TO splittings for the corresponding concentration, and $Z_{\mathrm{Al}}(x)$ is determined so as to satisfy the relation for the effective charge parameter of the alloy $\mathrm{Al}_x\mathrm{Ga}_{1-x}\mathrm{As}$, $Z_{\mathrm{Al}_x\mathrm{Ga}_{1-x}\mathrm{As}}(x)$, as

$$Z_{\mathrm{Al}_x\mathrm{Ga}_{1-x}\mathrm{As}}(x) = (1-x)Z_{\mathrm{Ga}}(x) + xZ_{\mathrm{Al}}(x) \tag{22}$$

$$= (1-x)Z_{\mathrm{GaAs}} + xZ_{\mathrm{AlAs}}, \tag{23}$$

where Z_{GaAs} and Z_{AlAs} are the effective charge parameters of the bulk materials given in Table I. The parameters obtained for $\mathrm{Al}_x\mathrm{Ga}_{1-x}\mathrm{As}$ are shown in Table II. The Ga-As or Al-As bond-stretching force constant increases with decreasing the corresponding cation concentration. The effective charge of Ga also increases with decreasing Ga concentration. A composition dependence of the bond-bending force constant is not introduced because its influence on optical branch is small compared to that of the bond-stretching term.

The calculated values of the long-wavelength GaAs- and AlAs-like optical-phonon frequencies of $\mathrm{Al}_x\mathrm{Ga}_{1-x}\mathrm{As}$ as functions of x are compared with the experimental values[25–27] in Fig. 2. It shows the expected two-mode behavior, AlAs-like modes at higher frequencies and GaAs-like modes at lower frequencies. Alloying lowers the longitudinal modes more than the transverse ones. The calculated frequencies agree quite well with most of the experimental values. The fit for the AlAs-like TO phonons is poorer because we fit the effective charge of the Ga only, not that of the Al ions.

TABLE II. Fit parameters for $\mathrm{Al}_x\mathrm{Ga}_{1-x}\mathrm{As}$ alloy system.

α^0_{GaAs}	α^0_{AlAs}	Z^0_{Ga}	θ_{GaAs}	θ_{AlAs}	λ_{Ga}
67.35	46.29	1.660	0.4628	0.2184	0.6

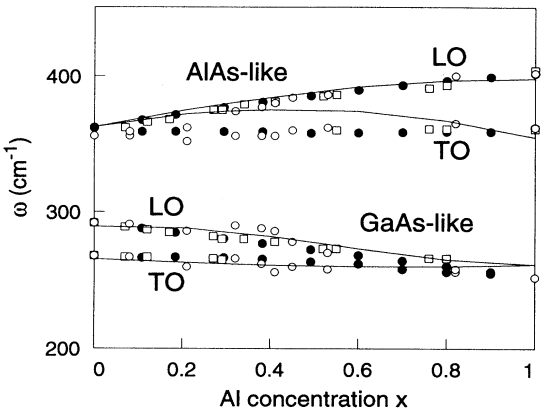

FIG. 2. Long-wavelength LO and TO phonon frequencies as functions of x in bulk $\mathrm{Al}_x\mathrm{Ga}_{1-x}\mathrm{As}$. The solid curves represent the results of the present calculation using the parameters of Table II. Experimental data points are indicated by circles (Ref. 25), squares (Ref. 26), and full circles (Ref. 27).

Figure 3 shows the phonon dispersion curves of a $(\mathrm{GaAs})_2/(\mathrm{Al}_{0.3}\mathrm{Ga}_{0.7}\mathrm{As})_2$ SL along the growth direction. The AlAs-like LO modes are shifted to lower frequencies and AlAs-like TO modes move to higher frequencies than the corresponding modes of the GaAs/AlAs SL shown in Fig. 1, which is consistent with the trend shown in Fig. 2. All AlAs-like optical modes are confined and dispersionless, whereas GaAs-like modes show different

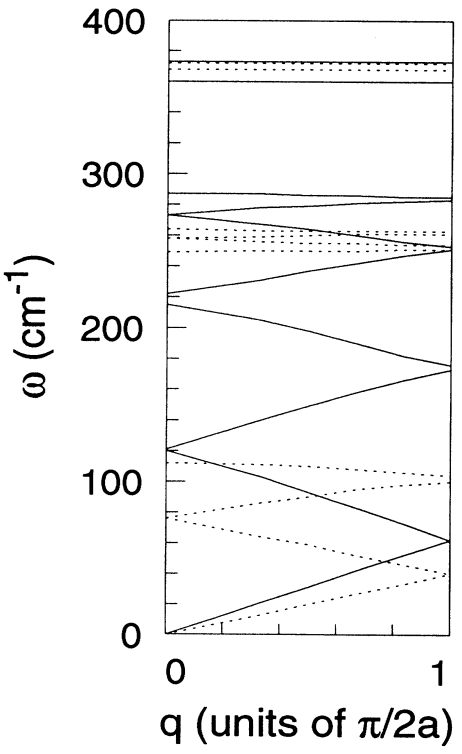

FIG. 3. Phonon dispersion curves for the $(\mathrm{GaAs})_2/(\mathrm{Al}_{0.3}\mathrm{Ga}_{0.7}\mathrm{As})_2$ SL along the growth direction. The solid (dotted) lines show longitudinal (transverse) modes.

features, owing to the presence of Ga ions in both layers of the $(GaAs)_2/(Al_{0.3}Ga_{0.7}As)_2$ SL. This is due to the fact that optical-phonon branches of bulk GaAs and $Al_{0.3}Ga_{0.7}As$ overlap below the top of the LO GaAs-like band of the alloy [which is lower than the LO(Γ) frequency of bulk GaAs]. In general, superlattice modes are expected to have extended or confined character, depending on whether their frequency is allowed for both constituents or just for one of them. By a naive application of this reasoning, dispersionless confined LO modes would be expected only between the top of the LO continua of the two materials. The rest of the GaAs-like LO phonons, whose frequencies fall in the overlap region, would be folded and dispersive. However, it has been noted that, even in the overlap regions, resonant modes may still exist, with significant displacement amplitude only in one of the constituents. These are called quasiconfined modes, to distinguish them from the proper confined modes, which result in the frequency range allowed for one of the two constituents only.[28] Although this quasiconfinement is not well pronounced in the $(GaAs)_2/(Al_{0.3}Ga_{0.7}As)_2$ SL case, it is clearly seen in longer-period SL's.

It has been reported that no microscopic interface modes can be formed in GaAs/AlAs SL's because there is no new atomic pair at the interface.[22,29] We were also unable to find interface modes along the growth [001] direction.[15] Nevertheless, there are some modes which show increasing localization at interfaces with increasing $q_{\|}$ and are identified as macroscopic interface modes. These interface modes and confined modes fall very close in frequency and thus mix strongly. Therefore, it is generally complicated to identify one of the GaAs (AlAs)-like phonons as an interface phonon near the zone center, without noting that macroscopic interface modes have large angular dispersion in the long-wavelength limit.[2,30] The contribution of these interface modes to the scattering rates is very important and will be discussed in the following.

IV. MICROSCOPIC CALCULATION OF *e*-ph SCATTERING RATES IN QW's WITH ALLOY CONSTITUENTS

We have calculated the scattering rates for Fröhlich-type electron–optical-phonon interaction in QW's, based on the above microscopic description of the phonon spectra. In a single QW, the potential $\varphi^{\nu}_{\mathbf{q}_{\|}}(z)$ associated with the quantized phonon mode ν, whose sth atomic displacement is $\mathbf{u}^{\nu}_{s}(\mathbf{q}_{\|})$, is given by

$$\varphi^{\nu}_{\mathbf{q}_{\|}}(z)=\sum_{s}\frac{-e^{*}_{s}}{2\Omega_{\|}\epsilon_{\infty}}\sqrt{\frac{\hbar}{2N_{\|}\omega^{\nu}_{s}(\mathbf{q}_{\|})}}\left(\frac{i\mathbf{q}_{\|}\cdot\mathbf{u}^{\nu}_{s}(\mathbf{q}_{\|})}{|\,\mathbf{q}_{\|}\,|}-u^{\nu}_{sz}(\mathbf{q}_{\|})\mathrm{sign}(z-r_{sz})\right)e^{-q_{\|}|z-r_{sz}|}e^{-i\mathbf{q}_{\|}\cdot\mathbf{r}_{s\|}}, \tag{24}$$

where e^{*}_{s} is the effective charge of the sth ion located at $\mathbf{r}_{s}$ in the unit cell, $\Omega_{\|}$ is the area of the two-dimensional unit cell, ϵ_{∞} is the high-frequency dielectric constant of the appropriate layer, and $N_{\|}$ is the number of lattice points in the normalization volume. Since performing a lattice-dynamical calculation is much easier for a system with three-dimensional periodicity, we simulate our GaAs QW within a supercell geometry, i.e., we extract the QW frequencies and displacements from the output of a SL calculation. The wave vectors $\mathbf{q}$ of interest for the calculation of the e-ph scattering in QW's have the largest component parallel to the interfaces because the electrons are confined in the well, and we choose $\mathbf{q}$ along the [100] direction. It is assumed that there is no dispersion of the optical mode frequencies along the [100] direction since the range of $\mathbf{q}_{\|}$'s involved in the transitions is limited.[2]

We consider two QW's, GaAs/AlAs and $GaAs/Al_{0.3}Ga_{0.7}As$, with the same well width of 56.5 Å. For $Al_xGa_{1-x}As$ materials, the barrier height $V(x)$ (in units of eV) and the optical dielectric constant $\epsilon_{\infty}(x)$ have, respectively, the forms[31,32]

$$V(x)=\begin{cases}1.247xf, & 0<x<0.45\\ [1.247x+1.147(x-0.45)^2]f, & 0.45<x<1.0,\end{cases} \tag{25}$$

$$\epsilon_{\infty}(x)=10.89-2.73x, \tag{26}$$

where f is the conduction-band offset parameter and, in general, is taken to be 0.65.

For the electron wave function, we use the solutions of Schrödinger's equation within the effective-mass approximation.[14] The envelope functions of the lowest subbands, 1 and 2, for both QW's are shown in Fig. 4. Of course, the electron wave functions of the $GaAs/Al_{0.3}Ga_{0.7}As$ QW, especially that of the second subband, are more extended than in the GaAs/AlAs QW. From the poor confinement of electron wave functions in the alloy system, we can easily see that the infinite barrier height approximation may introduce large errors in the calculation of the overlap integrals g_{ij}, and thus large errors in the calculation of scattering rates.[33,34]

In many quasi-two-dimensional situations, the scattering rates involving the two lowest subbands are most interesting. We first calculate the room-temperature emission rates for the 1→1 and 2→1 transitions in the GaAs/AlAs QW. In order to compare our results with those of Ref. 2, we use the same parameters as the ones they used ($e^{*}_{\mathrm{GaAs}}=2.07, e^{*}_{\mathrm{AlAs}}=2.17$). The results are shown in Fig. 5. Our total scattering rates are in excellent agreement with those of Ref. 2. Major contributions are from GaAs- and AlAs-like interface (IF) modes, and from the lowest-order confined mode with the appropriate symmetry as mentioned in Sec. II, namely, the first confined mode for the intrasubband scattering and the second confined mode for the intersubband scattering.

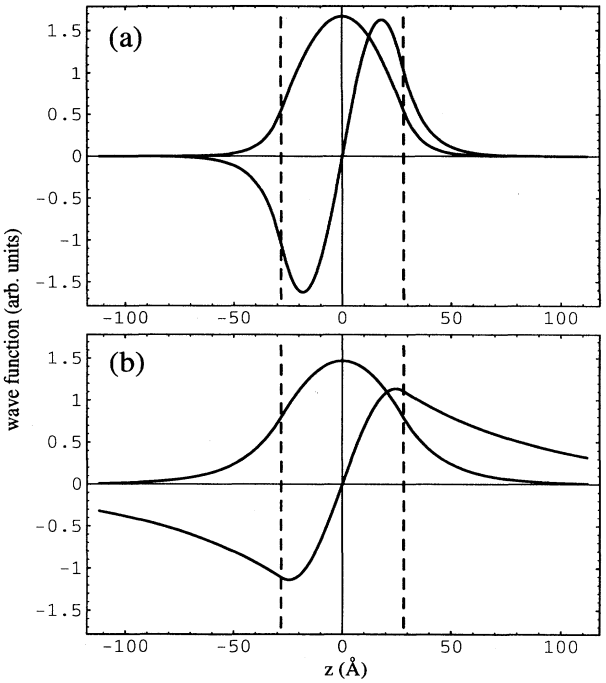

FIG. 4. Envelope functions of the two lowest electronic subbands for (a) the GaAs/AlAs and (b) GaAs/$Al_{0.3}Ga_{0.7}As$ QW's. The even (odd) function is for the subband 1 (2). The GaAs layer is centered at $z = 0$; the dashed vertical lines indicate the As interface planes.

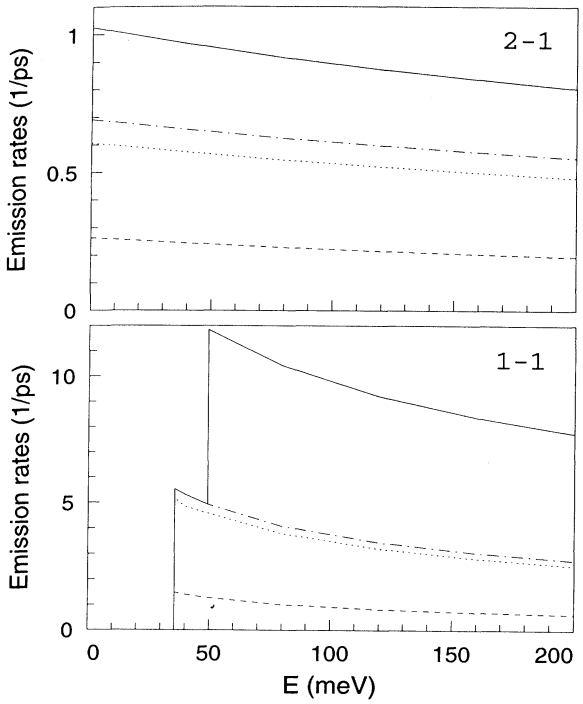

FIG. 5. Calculated total intersubband and intrasubband emission rates as a function of electron energy in the GaAs/AlAs QW including all GaAs- and AlAs-like optical modes (solid lines). The dashed-dotted lines show the contribution of all GaAs-like modes, out of which the lowest-order GaAs-like confined mode [first ($\omega = 288.5$ cm^{-1}) for intrasubband and second ($\omega = 287.7$ cm^{-1}) for intersubband transitions] and the GaAs-like interface mode ($\omega = 269.4$ cm^{-1} for intrasubband and $\omega = 265.4$ cm^{-1} for intersubband transitions) give the dominant contribution and are shown by the dashed and the dotted lines, respectively.

Interface (IF) modes give a larger contribution than confined modes as shown in Fig. 5. AlAs-like confined modes also contribute considerably, while their contribution is negligible in Ref. 2. To understand this result, we have to recall that—due to the artificially dispersive character of our LO branch of AlAs (see Sec. III)—confined modes fall close in energy to AlAs-like IF modes,[23] and, therefore, they mix strongly, similar to what happens in the GaAs-like range. This explains why, within our approximations, AlAs-like confined modes are also found to contribute to the scattering rates.

Figure 6 shows the room-temperature emission rates in the GaAs/$Al_{0.3}Ga_{0.7}As$ QW. AlAs-like mode contributions are considerably reduced because the Al mole concentration decreased from $x = 1$ to $x = 0.3$. However, for the intersubband transition they are still comparable to the case of the GaAs/AlAs QW, due to the fact that the second subband wave function is extended far into the barrier.

In the next section, we shall introduce a simple macroscopic model, the dielectric continuum model, which was shown to provide accurate results for e-ph scattering rates in the case of binary/binary structures.[2] After deriving its formulation for the case of ternary-semiconductor barriers, we shall compare its results with the outcome of our microscopic calculation.

V. MACROSCOPIC DCM CALCULATION OF e-ph SCATTERING RATES IN QW's WITH ALLOY CONSTITUENTS

In Ref. 2, macroscopic models were shown to be a very practical tool to obtain reliable estimates of e-ph rates, provided that they fulfill electrostatic interface boundary conditions (as is indeed the case for the DCM), and that appropriate input parameters are chosen to reproduce the vibrational properties of the constituent materials. We first review the formulation of the DCM,[1] give a detailed derivation of explicit normalized formulas and results for our prototype binary/ternary system, and verify their validity versus the microscopic scheme of the previous section.

Within the DCM, the semiconductors for the well (GaAs) and the barrier ($Al_xGa_{1-x}As$) are described by a dielectric function with poles at TO mode frequencies (ω_{TO}) and zeroes for the LO frequencies (ω_{LO}). The GaAs (material A) dielectric function is easily written as

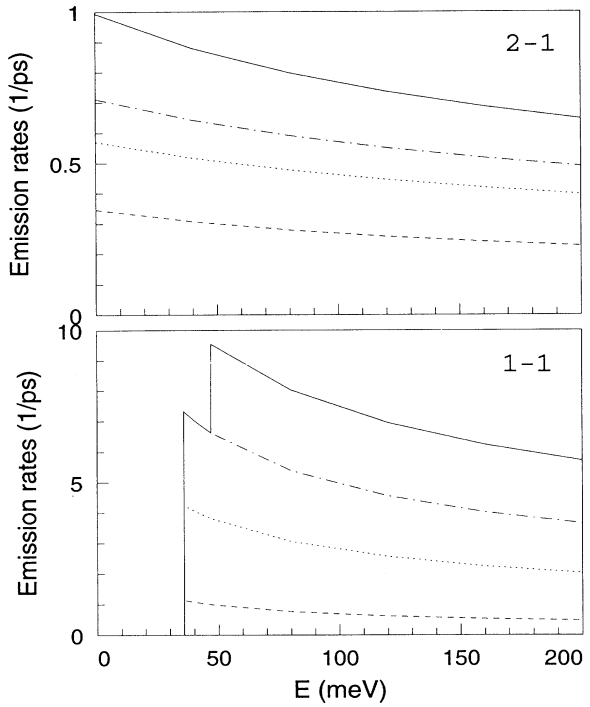

FIG. 6. Calculated total emission rates in a $GaAs/Al_{0.3}Ga_{0.7}As$ QW, including all GaAs- and AlAs-like optical modes (solid lines). The dashed-dotted lines show the contribution of all GaAs-like modes, out of which the lowest-order GaAs-like confined mode [first ($\omega = 288.6$ cm^{-1}) for intrasubband and second ($\omega = 288.2$ cm^{-1}) for intersubband transitions] and the GaAs-like interface mode ($\omega = 285.2$ cm^{-1} for intrasubband and $\omega = 265.2$ cm^{-1} for intersubband transitions) give the dominant contribution and they are shown by the dashed and the dotted lines, respectively.

$$\varepsilon_A(\omega) = \varepsilon_{\infty_A} \frac{\left(\omega^2 - \omega^2_{\mathrm{LO}_A}\right)}{\left(\omega^2 - \omega^2_{\mathrm{TO}_A}\right)}. \tag{27}$$

As concerns the alloy, of course the DCM has to reproduce the two-mode behavior, namely, the two distinct allowed frequency ranges corresponding to the vibration of Ga-As and Al-As bonds, respectively. This is easily obtained by writing the dielectric function for the alloy material $Al_xGa_{1-x}As$ (material B) in the two-pole form,

$$\varepsilon_B(\omega) = \varepsilon_{\infty_B} \frac{\left(\omega^2 - \omega^2_{L1_B}\right)\left(\omega^2 - \omega^2_{L2_B}\right)}{\left(\omega^2 - \omega^2_{T1_B}\right)\left(\omega^2 - \omega^2_{T2_B}\right)}, \tag{28}$$

where ω_{L1_B}, ω_{L2_B}, ω_{T1_B}, ω_{T2_B} are the LO and TO frequencies for GaAs-like and AlAs-like modes of the alloy at $\mathbf{q} = 0$. As discussed in Sec. III, these GaAs-like and AlAs-like branches will fall at frequencies which are lower than the corresponding bulk materials, and decrease with decreasing percentage of the appropriate cation. The two dielectric functions are shown in Fig. 7.

A detailed solution of the DCM for our case is presented in the Appendix. Several types of modes result, namely, GaAs confined modes in the well, AlAs-like and

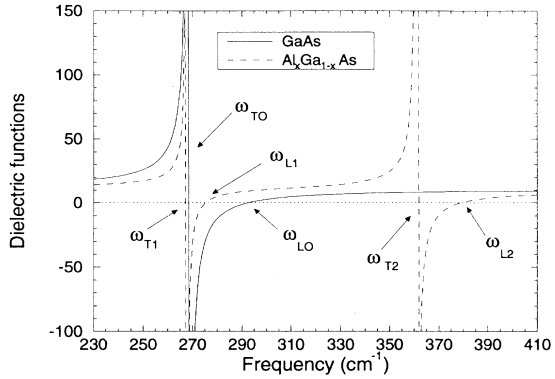

FIG. 7. One-pole and two-pole dielectric functions for GaAs and $Al_{0.3}Ga_{0.7}As$.

GaAs-like confined modes in the barrier, and IF modes. As shown by the frequency dispersions in Fig. 8, the IF modes include three branches, one AlAs-like and two GaAs-like, the latter being related to the frequencies of pure GaAs and of GaAs-like alloy vibrations. The corresponding potential profiles are displayed in Figs. 9–11.

In Fig. 12, we show results for emission rates as obtained from the two-pole DCM, and compare them with the corresponding data obtained within our microscopic model. The agreement is excellent both for the total rates and for the relative contribution of GaAs-like and AlAs-like modes, thus supporting the accuracy of the DCM also in the case of alloy-based systems.

Within the DCM, we also calculate the relative contribution of IF phonons to the scattering rate, which is found to increase as the well width L decreases. This is apparent in Fig. 13, where the $1 \rightarrow 1$ emission rate for Γ electrons is shown as a function of L. The rates are calculated at the threshold for the emission of an AlAs phonon, which corresponds to the peak value. For values of L smaller than 60 Å, the IF modes dominate, mainly be-

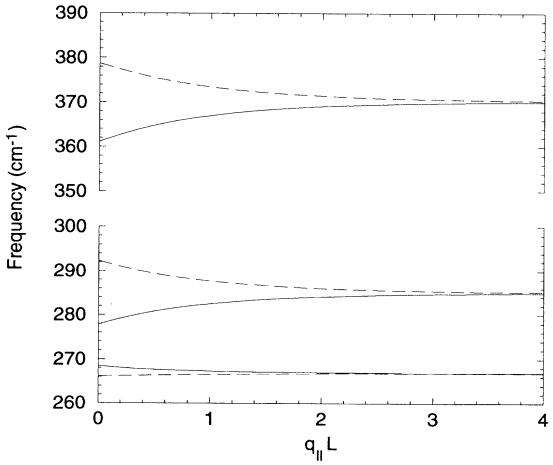

FIG. 8. Frequency dispersions of interface phonon modes calculated within the dielectric continuum model for a $GaAs/Al_{0.3}Ga_{0.7}As$ QW. Solid and dashed lines refer to symmetric and antisymmetric IF modes.

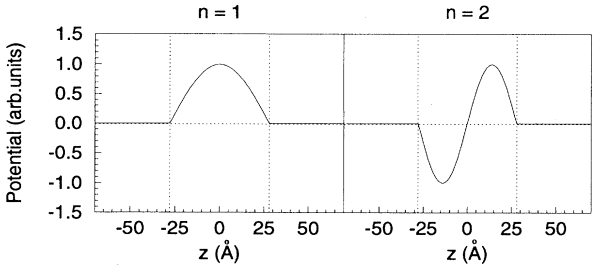

FIG. 9. Potential profile for the first ($n = 1$) and the second ($n = 2$) confined phonons in the well for a $GaAs/Al_{0.3}Ga_{0.7}As$ QW.

cause the quantized electronic levels are pushed at higher energies and the electron confinement decreases.

A similar effect occurs in the dependence of the scattering rate on the Al fraction in the $Al_xGa_{1-x}As$ alloy barrier, as presented in Fig. 14. As expected, when x gets smaller the AlAs contribution tends to disappear. On the contrary, high values of x imply strong scattering with AlAs-like phonons, in addition to the enhancement of the confined GaAs contribution due to the increased barrier height.

VI. CONCLUSIONS

We have presented calculations of the electron–optical-phonon interaction in GaAs/AlAs and GaAs/$Al_{0.3}Ga_{0.7}As$ QW's. A pseudo-unit-cell scheme is successfully utilized to derive the lattice-dynamical properties of $Al_xGa_{1-x}As$ alloy and alloy-based SLS. The contribution of individual modes to the scattering rates was examined. The results show that the lowest-order confined and the interface mode give the dominant contribution. To our knowledge, the present paper is the first work which calculates the electron–optical-phonon interaction in alloy systems based on a microscopic description of the phonon spectra. Our results for the emission rates in the alloy QW system support the two-pole dielectric continuum model calculations.

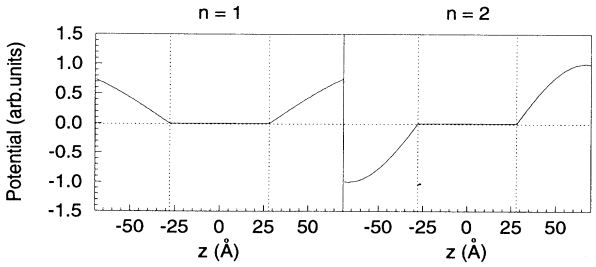

FIG. 10. Potential profile for the first ($n = 1$) and the second ($n = 2$) confined phonon modes in the barrier for a $GaAs/Al_{0.3}Ga_{0.7}As$ QW.

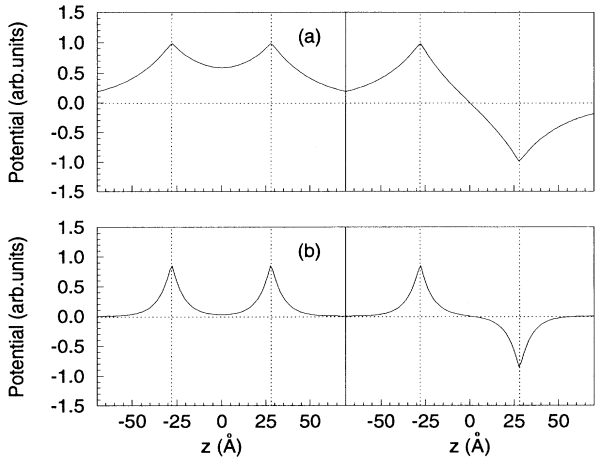

FIG. 11. Potential profile of symmetric and antisymmetric IF phonon modes in $GaAs/Al_{0.3}Ga_{0.7}As$ QW. (a) $q_{\|} = 0.04$ Å^{-1}, (b) $q_{\|} = 0.15$ Å^{-1}.

ACKNOWLEDGMENTS

We are grateful to C. Bungaro for useful discussions in the early stages of the DCM calculations. This work was supported by the National Science Foundation ECS-

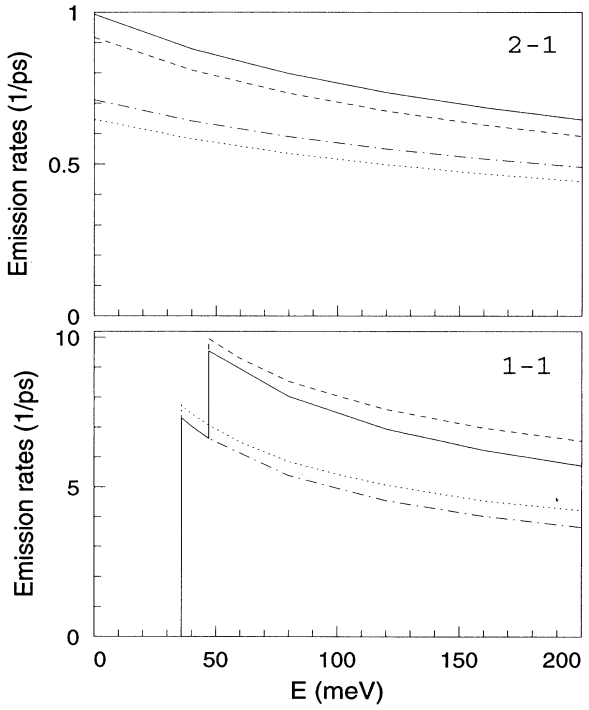

FIG. 12. Comparison of the emission rates from our microscopic model with the results of the two-pole dielectric continuum model. Solid lines represent the total scattering rates (GaAs- and AlAs-like modes) and dashed-dotted lines indicate the contribution of all GaAs-like modes. The corresponding results from the macroscopic model are shown by the dashed and the dotted lines, respectively.

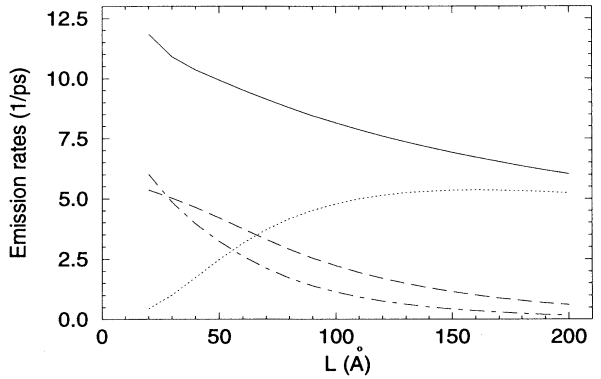

FIG. 13. Threshold emission rate vs well width for all modes in a $GaAs/Al_{0.3}Ga_{0.7}As$ QW (solid line). The dotted line refers to confined modes in the well, dashed and dashed-dotted lines show, respectively, the contribution of IF GaAs-like and AlAs-like modes.

8821107 and by the European Commission within the ESPRIT Project NANOPT and the HCM Network ULTRAFAST.

APPENDIX

In this appendix, we provide a detailed derivation of the dielectric continuum model and give the explicit normalized expressions of phonon potential and e-ph scattering rates for the general case of a quantum-well (material A) embedded in a barrier material (material B), which may be a ternary alloy. In this macroscopic approach, polar optical vibrations produce a macroscopic field, obtained from the solution of Laplace's equation in both materials,

$$\varepsilon_A(\omega)\,\nabla^2\varphi_A(\mathbf{r}) = 0 \qquad \text{(material } A\text{)}, \tag{A1}$$

$$\varepsilon_B(\omega)\,\nabla^2\varphi_B(\mathbf{r}) = 0 \qquad \text{(material } B\text{)}. \tag{A2}$$

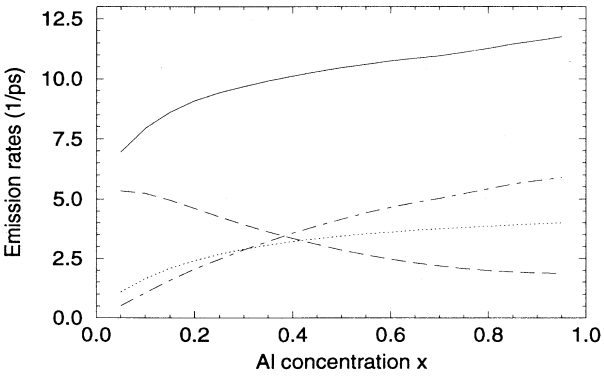

FIG. 14. Threshold emission rate as a function of the alloy composition x in a $GaAs/Al_xGa_{1-x}As$ QW (solid line). The dotted line refers to confined modes in the well, dashed and dashed-dotted lines show, respectively, the contribution of IF GaAs-like and AlAs-like modes.

Because of translational invariance in the direction parallel to the interfaces, the solutions are written in the form

$$\varphi(\mathbf{r},t) = \varphi(z)\,e^{i(\mathbf{q}_\parallel\cdot\mathbf{r}_\parallel-\omega t)}, \tag{A3}$$

and the boundary conditions at the interfaces will be

$$\begin{aligned} \varphi_A &= \varphi_B \qquad \text{(continuity of } E_\parallel\text{)}\,, \\ \varepsilon_A(\omega)\tfrac{\partial\varphi_A}{\partial z} &= \varepsilon_B(\omega)\tfrac{\partial\varphi_B}{\partial z} \quad \text{(continuity of } D_z\text{)}. \end{aligned}$$

From these equations, we get three types of phonon modes:

(i) Confined modes in the well when $\varepsilon_A = 0$.

(ii) Interface modes (IF) if both ε_A and ε_B are not zero.

(iii) Confined modes in the barrier when $\varepsilon_B = 0$.

The electrostatic potential $\varphi(\mathbf{r})$ will be a linear combination of "normal modes" (i.e., of solutions of equation $\varepsilon\,\nabla^2\varphi = 0$),

$$\varphi(\mathbf{r}) = \sum_{q_\parallel,\nu} f_\nu(q_\parallel)\,\Phi^\nu_{q_\parallel}(z)\,e^{i\mathbf{q}_\parallel\cdot\mathbf{r}_\parallel}\,(b+b^\dagger), \tag{A4}$$

where $f_\nu(q_\parallel)$ are the normalization coefficients. The electric field is then

$$\mathbf{E}(\mathbf{r}) = -\nabla\varphi(\mathbf{r}) = -\sum_{q_\parallel,\nu} f_\nu(q_\parallel)\,e^{i\mathbf{q}_\parallel\mathbf{r}_\parallel} \times\left(i\mathbf{q}_\parallel\,\Phi^\nu_{q_\parallel}\,,\hat{\mathbf{e}}_\mathbf{z}\frac{d}{dz}\Phi^\nu_{q_\parallel}\right)(b+b^\dagger). \tag{A5}$$

Following the Born-Huang approach,[35] the equation of motion in the binary material A (GaAs) can be written as

$$\mu_A\ddot{\mathbf{u}}(\mathbf{r}) = -\omega^2_{\mathrm{TO}_A}\mu_A\mathbf{u}(\mathbf{r}) + e^*_A\mathbf{E}(\mathbf{r}), \tag{A6}$$

where μ_A is the reduced mass of the ions, e^*_A the effective charge per unit cell, ω_{TO_A} the transverse frequency, $\mathbf{u}(\mathbf{r})$ the ionic displacement, and $\mathbf{E}(\mathbf{r})$ the local electric field. The effective charge is given by

$$e^{*^2}_A = \varepsilon_{\infty_A}\mu_A\Omega\left(\omega^2_{\mathrm{LO}_A} - \omega^2_{\mathrm{TO}_A}\right). \tag{A7}$$

In a ternary material B ($Al_xGa_{1-x}As$), there are two equations of motion,

$$\mu_{i_B}\ddot{\mathbf{u}}_i(\mathbf{r}) = -\omega^2_{Ti_B}\mu_{i_B}\mathbf{u}_i(\mathbf{r}) + e^*_{i_B}\mathbf{E}(\mathbf{r}), \tag{A8}$$

with $i = 1,2$ referred to GaAs-like and AlAs-like alloy modes. The polarization now depends on the contribution of both pairs of oscillating ions (Ga-As and Al-As),

$$\mathbf{P}(\mathbf{r}) = \frac{1}{\Omega}\left[e^*_{1_B}\mathbf{u}_1(\mathbf{r}) + e^*_{2_B}\mathbf{u}_2(\mathbf{r})\right]. \tag{A9}$$

Assuming a two-pole dielectric function (27) and using the Born-Huang equations, we get

$$e^{*^2}_{1_B} = \varepsilon_{\infty_B}\mu_{1_B}\Omega\left(\omega^2_{L1_B} - \omega^2_{T1_B}\right)\frac{\left(\omega^2_{L2_B} - \omega^2_{T1_B}\right)}{\left(\omega^2_{T2_B} - \omega^2_{T1_B}\right)}, \tag{A10}$$

$$e^{*^2}_{2_B} = \varepsilon_{\infty_B}\mu_{2_B}\Omega\left(\omega^2_{L2_B} - \omega^2_{T2_B}\right)\frac{\left(\omega^2_{L1_B} - \omega^2_{T2_B}\right)}{\left(\omega^2_{T1_B} - \omega^2_{T2_B}\right)}. \quad \text{(A11)}$$

Moreover, from Born-Huang equations (A8), the electric field is

$$\mathbf{E}^\nu(\mathbf{r}) = \frac{\mu_\lambda}{e^*_\lambda}(\omega^2_{T_\lambda} - \omega^2_\nu)\mathbf{u}^\nu(\mathbf{r}), \quad \text{(A12)}$$

where λ is referred to material A or the GaAs-like and the AlAs-like modes of barrier (in our notation it can be "A," "1_B," or "2_B," respectively).

Writing $\mathbf{u}^\nu(\mathbf{r})$ as

$$\mathbf{u}^\nu(\mathbf{r}) = \sum_{q_\parallel} \mathbf{u}^\nu(q_\parallel, z)\, e^{i\mathbf{q}_\parallel\cdot\mathbf{r}_\parallel} \quad \text{(A13)}$$

and using the standard quantization of displacements in normal modes

$$\mathbf{u}^\nu(q_\parallel, z) = \sqrt{\frac{\hbar\Omega}{2A\mu\omega_\nu}}\,\mathbf{v}^\nu(q_\parallel, z)\,(b + b^\dagger)\ , \quad \text{(A14)}$$

it follows that

$$\mathbf{E}(\mathbf{r}) = \sum_{q_\parallel,\nu}\frac{\mu_\lambda}{e^*_\lambda}(\omega^2_{T_\lambda} - \omega^2_\nu)\sqrt{\frac{\hbar\Omega}{2A\mu_\lambda\omega_\nu}} \times e^{i\mathbf{q}_\parallel\cdot\mathbf{r}_\parallel}\,\mathbf{v}^\nu_\lambda(q_\parallel, z)\,(b + b^\dagger). \quad \text{(A15)}$$

Comparing (A5) and (A15), we obtain the displacements

$$\mathbf{v}^\nu_\lambda(q_\parallel, z) = f_\nu(q_\parallel)\left(i\mathbf{q}_\parallel\,\Phi^\nu_{q_\parallel}, \hat{\mathbf{e}}_\mathbf{z}\frac{d}{dz}\Phi^\nu_{q_\parallel}\right) \times\sqrt{\frac{2A\mu_\lambda\omega_\nu}{\hbar\Omega}}\,\frac{e^*_\lambda}{\mu_\lambda(\omega^2_\nu - \omega^2_{T_\lambda})}. \quad \text{(A16)}$$

Finally, we can substitute (A16) in the normalization equation,

$$\int_A \left|\mathbf{v}^\nu_A(q_\parallel, z)\right|^2 dz + \int_B \left|\mathbf{v}^\nu_{1_B}(q_\parallel, z)\right|^2 dz + \int_B \left|\mathbf{v}^\nu_{2_B}(q_\parallel, z)\right|^2 dz = 1, \quad \text{(A17)}$$

and integrate, obtaining

$$f_\nu(q_\parallel) = \sqrt{\frac{\hbar\Omega}{2A\omega_\nu}}\left[\frac{e^{*^2}_A J_1}{\mu_A(\omega^2_\nu - \omega^2_{TO_A})^2} + \frac{e^{*^2}_{1_B} J_2}{\mu_{1_B}(\omega^2_\nu - \omega^2_{T1_B})^2} + \frac{e^{*^2}_{2_B} J_2}{\mu_{2_B}(\omega^2_\nu - \omega^2_{T2_B})^2}\right]^{-\frac{1}{2}}, \quad \text{(A18)}$$

with

$$J_1 = \int_A\left(q^2_\parallel\left|\Phi^\nu_{Aq_\parallel}(z)\right|^2 + \left|\frac{d\Phi^\nu_{Aq_\parallel}(z)}{dz}\right|^2\right)dz,$$

$$J_2 = \int_B\left(q^2_\parallel\left|\Phi^\nu_{Bq_\parallel}(z)\right|^2 + \left|\frac{d\Phi^\nu_{Bq_\parallel}(z)}{dz}\right|^2\right)dz.$$

The potential envelope $\Phi^\nu_{q_\parallel}(z)$ and the frequency ω_ν will depend on which mode (confined or IF) we want to evaluate.

(i) Confined modes in the well ($\varepsilon_A = 0, \varepsilon_B \neq 0$). From boundary conditions, solutions of Laplace's equation are $\Phi^\nu_B(z) = 0$ and

$$\Phi^\nu_A(z) = \begin{cases}\cos\left(\frac{\nu\pi z}{L}\right), & \nu \text{ odd}\\ \sin\left(\frac{\nu\pi z}{L}\right), & \nu \text{ even.}\end{cases} \quad \text{(A19)}$$

For these modes, using (A7) and taking into account that $\omega_\nu = \omega_{\mathrm{LO}}$ for each ν, the normalization coefficient from (A18) will be

$$f_\nu(q_\parallel) = \sqrt{\frac{\hbar}{2A}}\sqrt{\frac{\omega^2_{\mathrm{LO}} - \omega^2_{\mathrm{TO}}}{\omega_{\mathrm{LO}}\varepsilon_{\infty_A}}}\sqrt{\frac{2}{L}}\frac{1}{\sqrt{q^2_\parallel + \left(\frac{\nu\pi}{L}\right)^2}}. \quad \text{(A20)}$$

(ii) Interface modes ($\varepsilon_A \neq 0, \varepsilon_B \neq 0$). When $\varepsilon_A \neq 0$ and $\varepsilon_B \neq 0$, solutions of Laplace's equation,

$$\frac{d^2}{dz^2}\Phi^\nu_{q_\parallel}(z) = q^2_\parallel\,\Phi^\nu_{q_\parallel}(z), \quad \text{(A21)}$$

extend to both materials,

$$\Phi^\nu_{q_\parallel}(z) = \begin{cases}A_\nu e^{q_\parallel z}, & z \le -\frac{L}{2}\\ B_\nu e^{q_\parallel z} + C_\nu e^{-q_\parallel z}, & -\frac{L}{2} \le z \le \frac{L}{2}\\ D_\nu e^{-q_\parallel z}, & z \ge \frac{L}{2}.\end{cases} \quad \text{(A22)}$$

From boundary conditions at the interfaces, we get the dispersion relation ω vs $q_\parallel$ for these modes as solution of the equation:

$$\frac{1}{2}\left[\frac{\varepsilon_A(\omega)}{\varepsilon_B(\omega)} + \frac{\varepsilon_B(\omega)}{\varepsilon_A(\omega)}\right]\sinh(q_\parallel L) + \cosh(q_\parallel L) = 0. \quad \text{(A23)}$$

For a ternary barrier material like $\mathrm{Al}_x\mathrm{Ga}_{1-x}\mathrm{As}$, we obtain three pairs of branches (symmetric and antisymmetric): one of them lies in the region of AlAs-like frequencies and the others in the GaAs and GaAs-like regions. The dependence on the alloy composition is contained in the values of ε_{∞_B} and ω_{L1_B}, ω_{L2_B}, ω_{T1_B}, ω_{T2_B}.

The coefficients for the symmetric potential envelopes are

$$A_\nu = D_\nu = e^{q_\parallel L/2},$$

$$B_\nu = C_\nu = \frac{1}{2\cosh\frac{q_\parallel L}{2}},$$

and for the antisymmetric ones,

$$A_\nu = -D_\nu = e^{q_\parallel L/2},$$

$$B_\nu = -C_\nu = -\frac{1}{2\sinh\frac{q_\parallel L}{2}}.$$

Integrating the potential over z, from (A18), we obtain the normalization coefficients,

$$f_\nu(q_\parallel)=\sqrt{\frac{\hbar}{2A\omega_\nu}}\left[\varepsilon_{\infty_A}\frac{\omega^2_{\mathrm{LO}_A}-\omega^2_{\mathrm{TO}_A}}{(\omega^2_\nu-\omega^2_{\mathrm{TO}_A})^2}J_1 +\varepsilon_{\infty_B}\left(\frac{\omega^2_{L1_B}-\omega^2_{T1_B}}{(\omega^2_\nu-\omega^2_{T1_B})^2}\frac{\omega^2_{L2_B}-\omega^2_{T1_B}}{\omega^2_{T2_B}-\omega^2_{T1_B}} +\frac{\omega^2_{L2_B}-\omega^2_{T2_B}}{(\omega^2_\nu-\omega^2_{T2_B})^2}\frac{\omega^2_{L1_B}-\omega^2_{T2_B}}{\omega^2_{T1_B}-\omega^2_{T2_B}}\right)J_2\right]^{-\frac{1}{2}}, \quad \text{(A24)}$$

with

$$J_1=2q_\parallel\,(B^2_\nu+C^2_\nu)\sinh(q_\parallel L),$$

$$J_2=q_\parallel\,(A^2_\nu+D^2_\nu)e^{-q_\parallel L}\ .$$

(iii) Confined modes in the barrier ($\varepsilon_A\neq 0,\varepsilon_B=0$). Solutions of confined modes in the barrier are sine-like functions,

$$\Phi^\nu_{q_\parallel}(z)=\begin{cases}\sin\frac{\nu\pi}{B}\left(z+B+\frac{L}{2}\right), & z\le-\frac{L}{2}\\ 0, & -\frac{L}{2}\le z\le\frac{L}{2}\\ \sin\frac{\nu\pi}{B}\left(z-\frac{L}{2}\right), & z\ge\frac{L}{2},\end{cases} \quad \text{(A25)}$$

where B is the barrier width. Notice that there are confined modes in the barrier for both the longitudinal frequencies of the alloy, ω_{L1_B} and ω_{L2_B}.

With this potential the normalization coefficients will be

$$f_\nu(q_\parallel)=\sqrt{\frac{\hbar}{2A\omega_\nu\varepsilon_{\infty_B}}}\sqrt{\frac{2}{B}}\frac{1}{\sqrt{q^2_\parallel+\left(\frac{\nu\pi}{B}\right)^2}} \times\left(\frac{\omega^2_{L1_B}-\omega^2_{T1_B}}{(\omega^2_\nu-\omega^2_{T1_B})^2}\frac{\omega^2_{L2_B}-\omega^2_{T1_B}}{\omega^2_{T2_B}-\omega^2_{T1_B}} +\frac{\omega^2_{L2_B}-\omega^2_{T2_B}}{(\omega^2_\nu-\omega^2_{T2_B})^2}\frac{\omega^2_{L1_B}-\omega^2_{T2_B}}{\omega^2_{T1_B}-\omega^2_{T2_B}}\right)^{-\frac{1}{2}}, \quad \text{(A26)}$$

where ω_ν is the longitudinal frequency of GaAs-like or AlAs-like modes.

For each type of mode, the Hamiltonian for e-ph interaction can be written as

$$H_{e-\mathrm{ph}}(\mathbf{r})=-e\varphi(\mathbf{r}) =-e\sum_{q_\parallel,\nu}f_\nu(q_\parallel)\,\Phi^\nu_{q_\parallel}(z)e^{i\mathbf{q}_\parallel\cdot\mathbf{r}_\parallel}\,(b+b^\dagger), \quad \text{(A27)}$$

with $f_\nu(q_\parallel)$ and $\Phi^\nu_{q_\parallel}$ given by the appropriate equation for confined or interface modes.

For confined modes (in the well or the barrier), we have

$$\Gamma_{ij}(k_\parallel)=\frac{2\pi e^2}{\hbar}\frac{A}{(2\pi)^2}\sum_\nu\begin{pmatrix}n_{q\nu}+1\\ n_{q\nu}\end{pmatrix} \times C^\nu_{ij}\int d^2\mathbf{k}'_\parallel\frac{\delta\left(\frac{\hbar^2k'^2_\parallel}{2m^*}-\frac{\hbar^2k^2_\parallel}{2m^*}\pm\hbar\omega^*\right)}{q^2_\parallel+q^2_z}, \quad \text{(A28)}$$

where $q_z=\nu\pi/L$ for the well and $q_z=\nu\pi/B$ for the barrier, and

$$\frac{C^\nu_{ij}}{q^2_\parallel+q^2_z}=\int\xi^*_j(z)f_\nu(q_\parallel)\Phi^\nu_{q_\parallel}(z)\xi_i(z)dz. \quad \text{(A29)}$$

Using polar coordinates and after integration over all possible $k'_\parallel$ [see Eq. (1)] we get

$$\Gamma_{ij}(k_\parallel)=\frac{m^*Ae^2}{2\pi\hbar^3}\sum_\nu\begin{pmatrix}n_{q\nu}+1\\ n_{q\nu}\end{pmatrix}C^\nu_{ij}\int_0^{2\pi}\frac{d\theta}{2k^2_\parallel\mp\frac{2m^*\omega^*}{\hbar}+q^2_z-2k_\parallel\sqrt{k^2_\parallel\mp\frac{2m^*\omega^*}{\hbar}}\cos\theta}. \quad \text{(A30)}$$

Integrating over θ, for modes confined in the well we finally obtain

$$\Gamma_{ij}(k_\parallel)=\frac{m^*e^2}{2\pi\hbar^2}\frac{1}{L}\frac{\omega^2_{\mathrm{LO}_A}-\omega^{\mathrm{TO}_A}}{\omega_{\mathrm{LO}_A}\varepsilon_{\infty_A}}\begin{pmatrix}n_{q\nu}+1\\ n_{q\nu}\end{pmatrix}\sum_\nu\frac{\mathcal{F}^\nu_{ij}}{\sqrt{(2k^2_\parallel\mp\frac{2m^*\omega^*}{\hbar}+q^2_z)^2-2k^2_\parallel\left(k^2_\parallel\mp\frac{2m^*\omega^*}{\hbar}\right)}}, \quad \text{(A31)}$$

where

$$\mathcal{F}^\nu_{ij}=\left|\int dz\,\xi^*_j(z)\,\Phi^\nu_{q_\parallel}(z)\,\xi_i(z)\right|^2.$$

The same can be done for confined modes in the barrier using the appropriate normalization coefficients.

At last, according to Eq. (1), the scattering probabilities for interface modes will be

$$\Gamma_{ij}(k_\parallel)=\frac{m^*Ae^2}{2\pi\hbar^3}\sum_\nu\begin{pmatrix}n_{q\nu}+1\\ n_{q\nu}\end{pmatrix}\int_0^{2\pi}d\theta\mid g^\nu_{ij}(\sqrt{k'^2_0+k^2_\parallel-2k'_0k_\parallel\cos\theta})\mid^2, \quad \text{(A32)}$$

where

$$k_0' = \sqrt{k_{\parallel}^2 \mp \frac{2m^*\omega^*}{\hbar}} \tag{A33}$$

and the coupling factor g_{ij} is given by the overlap integral of the initial and final electronic state with the normalized IF phonon potential,

$$g_{ij}^{\nu}(q_{\parallel}) = \int \xi_j^*(z) f_{\nu}(q_{\parallel}) \Phi_{q_{\parallel}}^{\nu}(z) \xi_i(z) dz. \tag{A34}$$

[1] See, e.g., K. W. Kim and M. A. Stroscio, J. Appl. Phys. **68**, 6289 (1990), and references therein.

[2] H. Rücker, E. Molinari, and P. Lugli, Phys. Rev. B **45**, 6747 (1992); **44**, 3463 (1991).

[3] E. Molinari, S. Baroni, P. Giannozzi, and S. de Gironcoli, Phys. Rev. B **45**, 4280 (1992), and references therein.

[4] B. Jusserand, D. Paquet, and F. Mollot, Phys. Rev. Lett. **63**, 2397 (1989).

[5] S. Baroni, S. de Gironcoli, and P. Giannozzi, Phys. Rev. Lett. **65**, 84 (1990).

[6] M. Bernasconi and L. Colombo, Phys. Rev. B **43**, 14 447 (1991).

[7] R. Bonneville, Phys. Rev. B **24**, 1987 (1981).

[8] I. F. Chang and S. S. Mitra, Adv. Phys. **20**, 359 (1971).

[9] Insook Lee and S. M. Goodnick, Bull. Am. Phys. Soc. **38**, 810 (1993).

[10] F. Bechstedt, H. Gerecke, and H. Grille, Phys. Rev. B **47**, 13 540 (1993).

[11] F. Bechstedt, H. Grille, and R. Haupt, Phys. Rev. B **48**, 14 667 (1993).

[12] For a discussion on the validity of the choice of a scalar electrostatic potential in this context, see, e.g., P. A. Knipp and T. L. Reinecke, Phys. Rev. B **48**, 12 338 (1993).

[13] See, e.g., G. P. Srivastava, *The Physics of Phonons* (Hilger, New York, 1990).

[14] C. Weisbuch and B. Vinter, *Quantum Semiconductor Structures, Fundamentals and Applications* (Academic Press, San Diego, 1991), p. 13.

[15] Insook Lee and C. Y. Fong, Phys. Rev. B **44**, 6270 (1991).

[16] P. N. Keating, Phys. Rev. **145**, 637 (1966).

[17] S. Baroni, P. Giannozzi, and E. Molinari, Phys. Rev. B **41**, 3870 (1990).

[18] P. Giannozzi, S. de Gironcoli, P. Pavone, and S. Baroni, Phys. Rev. B **43**, 7231 (1991).

[19] G. S. Spencer, J. Grant, R. Gray, J. Zolman, J. Menéndez, R. Droopad, and G. N. Maracas, Phys. Rev. B **49**, 5761 (1994).

[20] J. Wagner, A. Fischer, W. Braun, and K. Ploog, Phys. Rev. B **49**, 7295 (1994).

[21] A. A. Maradudin, E. W. Montroll, G. H. Weiss, and I. P. Ipatova, in *Solid State Physics: Theory of Lattice Dynamics in the Harmonic Approximation*, 2nd ed., edited by F. Seitz, D. Turnbull, and H. Ehrenreich (Academic, New York, 1971), Suppl. 3.

[22] B. Jusserand and M. Cardona, in *Light Scattering in Solids V*, edited by M. Cardona and G. Güntherodt (Springer, Berlin, 1989), and references therein.

[23] As a consequence of the above-mentioned approximation in the AlAs force constants and the overestimated bulk AlAs LO dispersion, the confinement-induced shift of AlAs-like SL LO modes is also overestimated. See, for comparison, Ref. 3; see, also, Fig. 8 of E. Molinari, S. Baroni, P. Giannozzi, and S. de Gironcoli, in *Light Scattering in Semiconductor Structures and Superlattices*, edited by D. J. Lockwood and J. F. Young (Plenum, New York, 1991).

[24] S. C. Varshney, J. F. Vetelino, S. S. Mitra, and I. F. Chang, Phys. Rev. B **12**, 5912 (1975).

[25] M. Ilegems and G. L. Pearson, Phys. Rev. B **1**, 1576 (1970).

[26] B. Jusserand and A. J. Sapriel, Phys. Rev. B **24**, 7194 (1981).

[27] Z. C. Feng, S. Perkowitz, D. K. Kinell, R. L. Whitney, and D. N. Talwar, Phys. Rev. B **47**, 13 466 (1993).

[28] A. Fasolino, E. Molinari, and J. C. Maan, Phys. Rev. B **39**, 3923 (1989).

[29] Y. Liu and B. J. Inkson, Semicond. Sci. Technol. **4**, 1167 (1989).

[30] F. Bechstedt and H. Gerecke, Phys. Status Solidi B **154**, 565 (1989).

[31] H. C. Casey, Jr. and M. B. Panish, *Heterostructure Lasers* (Academic, New York, 1978), Part A.

[32] S. Adachi, J. Appl. Phys. **58**, R1 (1985).

[33] S. Rudin and T. L. Reinecke, Phys. Rev. B **41**, 7713 (1990).

[34] W. Duan, J. Zhu, and B. Gu, J. Phys. Condens. Matter **5**, 2859 (1993).

[35] M. Born and K. Huang, *Dynamical Theory of Crystal Lattices* (Oxford University Press, Oxford, 1954).